

A New Active Anti-Vibration System Using a Magnetostrictive Bimetal Actuator

Mojtaba Ghodsi^a, Morteza Mohammadzaheri^{b,c}, Payam Soltani^b, Hamidreza Ziaifar^c,

^a School of Energy and Electronic Engineering, University of Portsmouth, UK (corresponding author, phone: +44 (0) 23 9284 2674; e-mail: mojtaba.ghodsi@port.ac.uk; moj.ghodsi@gmail.com)

^b School of Engineering and the Built Environment, Birmingham City University, UK

^c Mechanical and Industrial Engineering Department, School of Engineering, Sultan Qaboos University, Oman School of

Abstract

This paper introduces a new vibration reduction system using a magnetostrictive (Fe-Ga alloy) bimetal actuator. The proposed method (i) uses a magnetostrictive bimetal actuator instead of prevalent single material ones that need an auxiliary temperature control system and (ii) utilises a novel disturbance rejection control scheme that eliminates an unknown disturbance, without needing knowledge of its dynamics. In experiments, the vibration source is demonstrated as an unbalanced motor attached to the tip of a cantilever beam, resembling a beam-like element subject to ambient vibrations. In the first step, the fundamental of this anti-vibration system is introduced and described. Then, analytical and data-driven modelling for the combination of the beam, the motor, and the bimetal is reported. These follow by model validation and impulse response analysis. Then, the proposed control system is introduced in detail. Experimental results indicate that the control system results in 33.6% decrease in beam vibration amplitude. Furthermore, the presented method in this paper can be employed as a design guideline for future applications.

Keywords: Active control, Magnetostrictive bimetal, Galfenol (Fe-Ga), Feedforward control, System identification.

Nomenclature

a	Input current amplitude
k	Constant coefficient
l_b	Position of an applied force by bimetal
l_d	Position of laser point
l_r	Position of an applied force by unbalanced rotating
m	Beam mass
m_0	Unbalanced mass
m_{eq}	Equivalent mass
p	Applied force by unbalanced rotating
q	Applied force by bimetal
r_{int}	Internal damping coefficient
r_{ext}	External damping coefficient
w	Displacement in the y-direction
(M_1, M_2)	Constant coefficients
E	Young Modulus
G	Green function
I	Moment of inertia
L	Total length of the cantilever beam
K	Spring coefficient
N	Bimetal coil's turns
M	Output tip displacement
M_m	Unbalanced rotating
P	Nominator coefficient of transfer function
P_0	Amplitude of Applied force by unbalanced rotating
Q_0	Amplitude of applied force by bimetal
T_d	Period of damped vibration
X_p	Tip displacement made by unbalanced rotating in the y-direction
X_q	Tip displacement made by bimetal in the y-direction

Greek symbol

ω	The rotational velocity of unbalanced rotating
ω_n	Natural frequency of cantilever beam
ω_d	Damped frequency of cantilever beam
δ	Logarithmic decrement
ζ	The damping ratio of beam
ξ	Damping ratio in the Transfer function
μ	The effective mass of magnetostrictive bimetal per unit length
μ^σ	Relative magnetic permeability
ϕ	The phase difference between input and output

1. Introduction

Unwanted vibrations are the most undesirable phenomena in many applications. Active control of the vibration in the flexible structures plays a significant role in their performance. For example, precise motion in a flexible robotic manipulator [1-4], suspension systems[5], noise cancellation[6], machining process [7, 8], and positioning of mirrors in the next generation of space telescope [9] are the most prominent applications of active control systems to eliminate or diminish these unwanted troublesome vibrations.

An appropriate actuator is an essential main component of any effective active vibration control system. Actuators made of smart materials are more compact, reliable, and have higher response speed compared to conventional actuators (such as hydraulic, pneumatic, electromagnetic, and electrostatic ones). Shape memory alloys, magnetorheological, piezoelectric, and magnetostrictive materials are the most representative smart materials in vibration attenuating systems. Shape memory alloy (SMA) is one of the promising smart materials for passive and active anti-vibration systems in mechanical and civil structures [10]. Many researchers employed SMA to attenuate the generated disturbances of a gimbal-type antenna of satellites [11-13] or gimbal camera stabilizer [14]. Compactness and high-strain combined with the lightweight make SMA very applicable in vibration control systems. However, its hysteresis behaviour, low-frequency response time, and high sensitivity to environmental thermal disturbances impose reservations on the use of this material. Magnetorheological materials in which their damping coefficient changes with the magnetic field are suitable candidates for semi-active control systems [15-17] and passive damping systems [18]. Despite high energy density and large generated force, magnetorheological material suffers from a low-frequency response and large required space for its drive system. Rapid development on flexible piezo elements since 2010 encouraged many researchers to employ piezo elements patches for a wide range of vibration control systems. For instance, piezo-actuated active control systems were employed in machining [19], wind turbines [20] and robot manipulators [21], and semi-active ones in automobile suspension systems [22]. Furthermore, different configurations of passive attenuation systems using shunted piezoelectric elements were reported [23-26]. Some researchers propose finite element models for the active vibration mechanism [27] or used the genetic algorithm to optimize the location and orientation of piezo sensors and actuators in active vibration control of planes [28]. Although the high-frequency response of piezoelectric patches are appropriate in medium-range temperature (i.e. 75-200 °C) [29, 30], and they are affordable [31, 32], low coupling efficiency, depolarization issue, and development of micro-cracks over time make their lifetime short and unviable in long-life applications [33].

Among all available smart materials used as actuators in an active vibration control system, magnetostrictive materials are the only candidate that performs well in harsh environments with high energy density [34, 35]. By discovering giant magnetostrictive materials (GMMs), especially Terfenol-D, in the 1970s, many researchers tried to model its Hysteresis behavior [36-38]. GMMs were employed for different applications such as sensors [39, 40], energy harvesters, and actuators [41, 42] including actuators in active vibration control of structures [43, 44]. As an instance of the latter application, Geng employed Terfenol-D to develop a six-degree-of-freedom (DOF) Stewart platform that can successfully attenuate vibrations up to 30 dB [45].

Despite all advantages of single-metal magnetostrictive actuators, their strain is influenced by two sources 1) magnetic field 2) thermal expansion due to generated heat by excitation coil or environment's temperature. To compensate for the thermal strain, it is required to use a temperature sensor along with a control system [46, 47]. In other words, the single-metal magnetostrictive actuator needs recalibration when it is used to operate in an

environment with a temperature different from standard temperature. To resolve these drawbacks, for the first time, in 1969, Nayman employed a magnetostrictive bimetal actuator (instead of a single-metal magnetostrictive actuator) to control devices [48] and other researchers employed it to develop sensors, actuators, and harvesters[34, 41, 49, 50]. As a significant advantage, the bimetal actuator (i.e., composed of two ferromagnetic layers with very close thermal expansion coefficients) practically does not witness the aforementioned thermal strain operating in a wide range of operational temperatures. Hence, there is no need for a temperature control system or any soft/hardware recalibration system anymore, which makes the control system simpler and more affordable [51]. The vibration of tools in lathe machine (i.e., chatter problem), the vibration of a manipulator in pick/place robots, and vibration of the mirror in the next generation of the space telescope in cryogenic conditions can be controlled by our proposed mechanism. All of these structures can be simplified as a cantilevered beam fixed under forced vibration condition. As a matter of novelty, this paper presents:

- i) an active vibration system that attenuates the vibration of a cantilever beam operating without using temperature sensor or any recalibration process.
- ii) a control scheme, which rejects the effect of any unknown disturbance, without the need for any knowledge of its dynamics.

2. Structure of the Proposed Control System

2.1. Principle of Operation

In this research, the active anti-vibration system is made of two main physical parts (i) a sensing component and (ii) the actuating component. As shown in Fig. 1, the proposed system controls the vibration of a Nickel cantilever beam excited by a rotating unbalance motor at its tip. The sensing component is a laser displacement sensor detecting the vibration of the tip of the beam. This sensing element operates based on the triangular optical beam using a position-sensitive detector (PSD). The actuation component is a magnetostrictive bimetal beam that acts against the excited vibration and attenuates the amplitude of the vibration generated by the rotating unbalance mass. The actuation part consists of a permanent magnet (PM), bimetal, excitation coil, and Nickel beam that makes a closed-magnetic circuit. As shown in Fig.2, the bimetal is a composite metal comprising of two or more metallic layers with a different magnetostrictive coefficient which bends when subjected to a magnetic field [34].

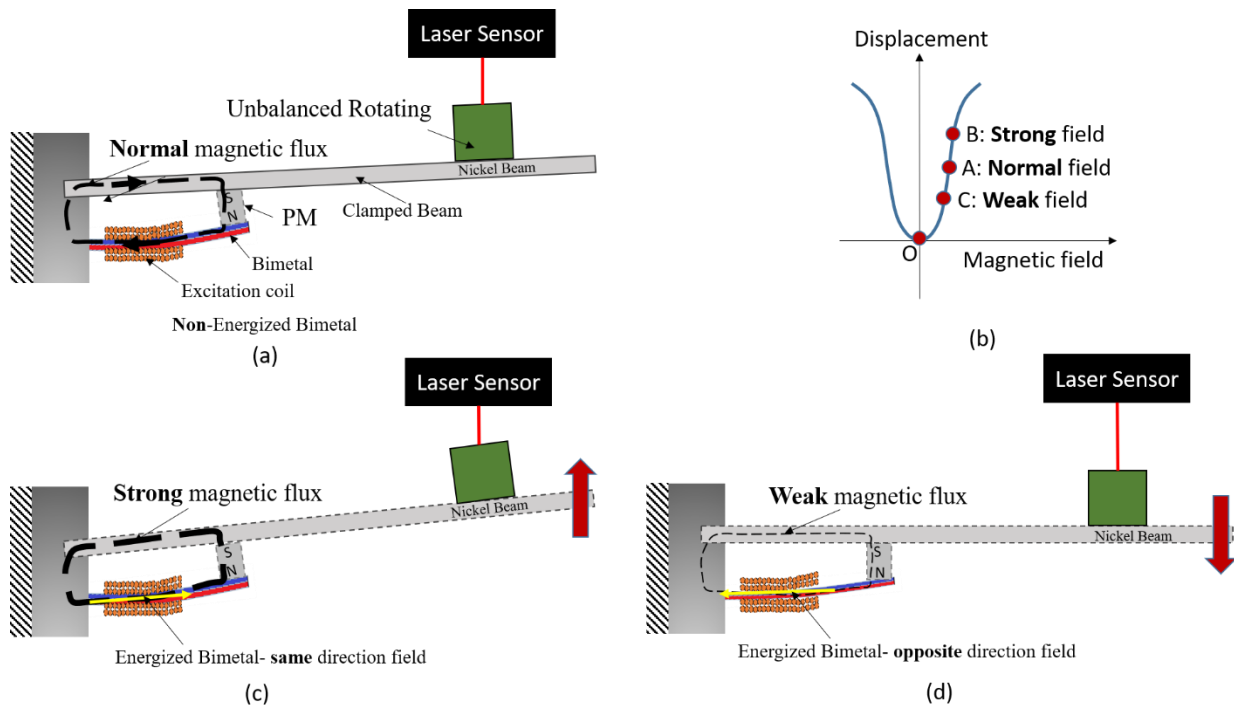


Fig. 1. Schematic of the proposed active anti-vibration system (a) non energized bimetal (normal field) (b) effect of magnetic bias on displacement-magnetic field curve (c) energized field is at the same direction of magnetic field (strong resultant magnetic field) (d) energized field is in the opposite direction of magnetic field (weak resultant magnetic field)

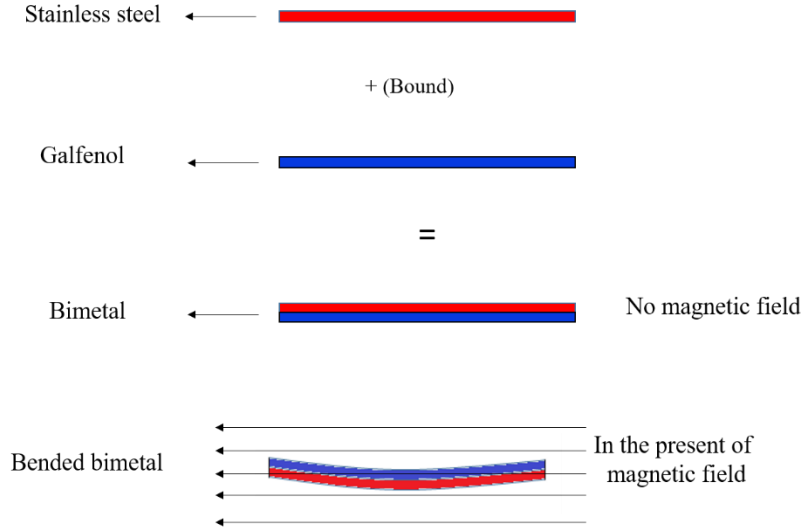


Fig.2. Principle of magnetostrictive bimetal [34]

The bimetal used in this research is composed of two strips: the Galfenol strip (Iron-Gallium alloy) and the non-ferromagnetic stainless steel strip (SUS 316) with approximately the same thermal expansion coefficient ($\approx 10 \times 10^{-6}/^\circ\text{C}$). The strips are bonded to each other by epoxy glue. The model and performance of the developed bimetal will be investigated in the following sections. Employing PM in the magnetic circuit has two main merits. The first is that it helps to increase the tip displacement range of the cantilever beam and keep the frequency of excitation and displacement equal. The next one is using the linear part of the displacement-field curve. Fig.1a shows a closed-loop magnetic field generated by the PM in the circuit. This magnetic bias will shift the operating point of the actuator to one side of the displacement-field curve. For example, the operating point shifts from O to A (Fig.1b). Assume the positive current generates a magnetic field with the same direction of PM's field and moves point A to B . Having a strong field causes upward displacement at the tip of the cantilever beam (Fig.1c). The negative current weakens the PM's field to provide downward displacement at the tip of the beam from B to A and C .

2.1. Analytical Modelling of a Beam Subject to the Proposed Control System

As explained in the previous section, the cantilever beam (Fig. 3) which is vibrating by an unbalanced rotating force $p(t)$, is controlled by the proposed control system. The deflection of the beam at vibrating end $x = l_d$ is measured by the laser sensor. A bimetal actuator applies the counteracting force, $q(t)$. The cantilever beam is realistically considered as a uniform Euler-Bernoulli beam, which has only vertical transverse vibration (the effects of shear deformation and rotary inertia of the beam are negligible). The applied force generates a moment on the magnetostrictive bar. The absolute displacement of the beam can be presented as [50]:

$$EI \frac{\partial^4 v(x, t)}{\partial x^4} + \mu \frac{\partial^2 v(x, t)}{\partial t^2} + r_{ext} \frac{\partial v(x, t)}{\partial t} + r_{int} \frac{\partial^5 v(x, t)}{\partial x^4 \partial t} = q(x, t) + p(x, t), \quad (1)$$

where $v(x, t)$ is the vertical displacement of the beam at the point x in the y -direction at time t . Furthermore, two damping factors are separately considered in this research. First, external damping factor, r_{ext} , which is influenced by the environment (e.g. air damping) and the internal damping, r_{int} , factor, or strain-rate independent damping (SRID), defined based on the theory of energy dissipation in solid media due to internal friction. Assuming that the applied oscillating forces to the cantilever beam are harmonic, they can be presented as:

$$\begin{aligned} p(x, t) &= P_0 e^{j\omega t} \delta(x - l_r), \\ q(x, t) &= Q_0 e^{j\omega t} \delta(x - l_b). \end{aligned} \quad (2)$$

Since the damping factors are considered in Eq. (1), the displacement of the beam, v , is considered to be complex. Therefore, Eq. (1) can be written as Eq. (3).

$$EI \frac{\partial^4 w(x, t)}{\partial x^4} + \mu \frac{\partial^2 w(x, t)}{\partial t^2} + r_{ext} \frac{\partial w(x, t)}{\partial t} + r_{int} \frac{\partial^5 w(x, t)}{\partial x^4 \partial t} = Q_0 e^{j\omega t} \delta(x - l_b) + P_0 e^{j\omega t} \delta(x - l_r) \quad (3)$$

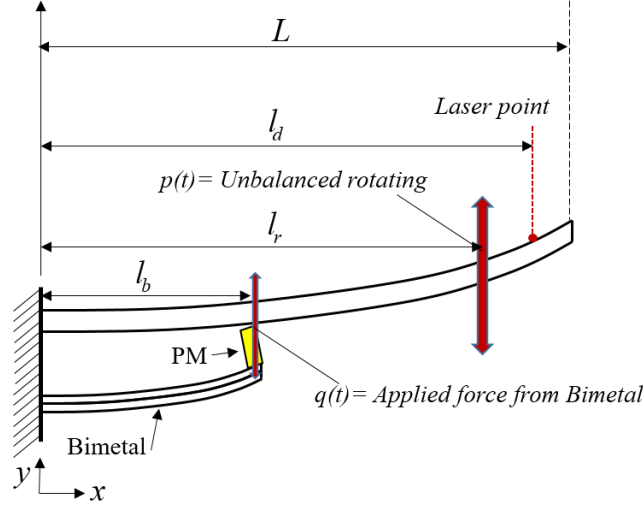


Fig. 3. Schematic of the proposed active vibration system

where $v(x,t)=\text{Re}\{w(x,t)\}$ Eq. (3) is a partial differential equation, and its solution is defined as using variable separation assumption [43]:

$$w(x, t) = X(x)T(t) = X(x)e^{j\omega t} . \quad (4)$$

By substituting Eq. (4) in Eq. (3):

$$\frac{\partial^4 X(x)}{\partial x^4} + \frac{(\mu\omega^2 - jr_{ext}\omega)}{(EI + jr_{int}\omega)} X = \frac{P_0 \delta(x - l_r)}{(EI + jr_{int}\omega)} + \frac{Q_0 \delta(x - l_b)}{(EI + jr_{int}\omega)} \quad (5)$$

Considering the superposition principle, the solution of the Eq. (5) is equal to the sum of the particular solutions for the following equations:

$$\frac{\partial^4 X(x)}{\partial x^4} + \frac{(\mu\omega^2 - jr_{ext}\omega)}{(EI + jr_{int}\omega)} X = \frac{P_0 \delta(x - l_r)}{(EI + jr_{int}\omega)}, \quad (6)$$

$$\frac{\partial^4 X(x)}{\partial x^4} + \frac{(\mu\omega^2 - jr_{ext}\omega)}{(EI + jr_{int}\omega)} X = \frac{Q_0 \delta(x - l_b)}{(EI + jr_{int}\omega)}. \quad (7)$$

The solution of Eq. 6, X_p can be found by Green function as:

$$X_p(x) = \int_0^{l_d} f(l_r) G(x, l_r) dl_r , \quad (8)$$

Green function in Eq. (8), $G(x, l_r)$, is the response of the beam to a unit force. Therefore, Eq. (5) should be rewritten in this form:

$$\frac{\partial^4 X(x)}{\partial x^4} + \frac{(\mu\omega^2 - jr_{ext}\omega)}{(EI + jr_{int}\omega)} X = \frac{\delta(x - l_r)}{(EI + jr_{int}\omega)}. \quad (9)$$

Applying the Laplace transform to Eq. (9), and solving the resultant in s (Laplace variable) domain leads to :

$$\hat{X}_p(s) = \frac{1}{(s^4 - k^4)} \left[\frac{e^{-slr}}{(EI + jr_{int}\omega)} + s^3 X(0) + s^2 X'(0) + sX''(0) + X'''(0) \right], \quad (10)$$

where (') demonstrates derivative against x and

$$k^4 = \frac{(\mu\omega^2 - jr_{ext}\omega)}{(EI + jr_{int}\omega)}. \quad (11)$$

Eq. (10) includes four unknowns. The boundary conditions of the beam are employed to reduce these unknowns to two. The cantilever beam is fixed in one end ($x=0$), so the displacement and the slope (derivation of the displacement) are zero at this end. At the other end of the beam ($x=L$), the beam is free and there are no bending moments and shearing force at this end:

$$x = 0 \Rightarrow \begin{cases} X(0) = 0, \\ X'(0) = 0, \end{cases} \quad (12)$$

$$x = L \Rightarrow \begin{cases} X''(L) = 0, \\ X'''(L) = 0. \end{cases} \quad (13)$$

By employing these boundary conditions, the inverse Laplace transform of Eq. (10) is written as:

$$X_p(x, l_r) = \frac{1}{2} \left[\frac{(\sinh k(x - l_r) - \sin k(x - l_r))u(x - l_r)}{k^3(EI + jr_{int}\omega)} + \frac{\cosh k(x - l_r) - \cos k(x - l_r)}{k^2} X''(0) + \frac{\sinh k(x - l_r) - \sin k(x - l_r)}{k^3} X'''(0) \right], \quad (14)$$

where $u(x - l_r)$ is a unit step function and $X''(0)$ and $X'''(0)$ are values of derivatives of the function X_p at position $x=0$. To calculate these variables, the derivation of function $X(x, l_r)$ are needed:

$$X''(x, l_r) = \frac{1}{2} \left[\frac{(\sinh k(x - l_r) + \sin k(x - l_r))}{k(EI + jr_{int}\omega)} + (\cosh k(x - l_r) + \cos k(x - l_r)) X''(0) + \frac{\sinh k(x - l_r) + \sin k(x - l_r)}{k} X'''(0) \right] \quad (15)$$

$$X'''(x, l_r) = \frac{1}{2} \left[\frac{(\cosh k(x - l_r) + \cos k(x - l_r))}{EI + jr_{int}\omega} + k(\sinh k(x - l_r) - \sin k(x - l_r)) X''(0) + (\cosh k(x - l_r) + \cos k(x - l_r)) X'''(0) \right] \quad (16)$$

By substituting Eq. (15) and Eq. (16) in (14), $X(x, l_r)$, can be obtained. Since $X(x, l_r)$ represents the green function of Eq. (8), we have:

$$\begin{aligned} & G(x, l_r) = X(x, l_r) \\ & = \frac{1}{2k^3(EI + jr_{int}\omega)} [(\sinh k(x - l_r) - \sin k(x - l_r)) u(x - l_r) \\ & + M_1((\sinh k(x - l_r) - \sin k(x - l_r)) u(x - l_r)) + M_2((\cosh k(x - l_r) + \cos k(x - l_r))], \end{aligned} \quad (17)$$

where

$$\begin{aligned}
& \frac{M_1}{=} \frac{(\sinh(L) - \sin(L))(\sinh(L - l_r) + \sin(L - l_r)) - (\cosh(L) + \cos(L))(\cosh(L - l_r) + \cos(L - l_r))}{(\cosh(L) + \cos(L))^2 - (\sinh(L) + \sin(L))(\sinh(L) - \sin(L))} \\
& \frac{M_2}{=} \frac{(\sinh(L) + \sin(L))(\cosh(L - l_r) + \cos(L - l_r)) - (\cosh(L) + \cos(L))(\sinh(L - l_r) + \sin(L - l_r))}{(\cosh(L) + \cos(L))^2 - (\sinh(L) + \sin(L))(\sinh(L) - \sin(L))}
\end{aligned} \tag{18}$$

since Green function, $G(x, l_r)$, is known, $G(x, l_r)$ can be substituted into Eq. (8) and $X_p(x)$ is found:

$$\begin{aligned}
X_p = \frac{1}{2k^3(EI + jr_{int}\omega)} \int_0^{l_d} & (\sinh k(x - l_r) - \sin k(x - l_r)) u(x - l_r) \\
& + M_1((\sinh k(x - l_r) - \sin k(x - l_r)) u(x - l_r)) + M_2((\cosh k(x - l_r) \\
& + \cos k(x - l_r)) f(l_r)) dl_r.
\end{aligned} \tag{19}$$

Similar approach is being followed to find the solution of Eq. (7) $X_q(x)$:

$$\begin{aligned}
X_q = \frac{1}{2k^3(EI + jr_{int}\omega)} \int_0^{l_d} & (\sinh k(x - l_b) - \sin k(x - l_b)) u(x - l_b) \\
& + M_1((\sinh k(x - l_b) - \sin k(x - l_b)) u(x - l_b)) + M_2((\cosh k(x - l_b) \\
& + \cos k(x - l_b)) f(l_b)) dl_r.
\end{aligned} \tag{20}$$

and by adding up X_p and X_q , resultant displacement X is finally concluded as:

$$X = X_p + X_q \tag{21}$$

2.2. Numerical Analysis of the Magnetic Circuit using Finite Element Method (FEM)

To analyse the magnetic circuit of the developed anti-vibration system, a 2D model is employed to show the magnetic flux with and without coil excitation in the presence of magnetic bias. The 2D model of the system with 5416 nodes is created based on six areas of Iron, Nickel, bimetal, air, PM, and coil. The areas mesh with element PLANE13 in ANSYS software (Fig. 4). Table 1 shows the characteristics of items employed in the model's areas. Figure 5 shows the 2D flux distribution of the anti-vibration system with the closed-magnetic circuit generated by PM, Nickel cantilever beam, iron support, and bimetal surrounded by the coil. Figure 5a depicts the magnetic flux generated only by the PM when the coil is not energized. After energizing the bimetal's coil, if the generated field is in the same direction as the PM's field, a strong field will be generated (Fig.5b). The PM's field will be weakened when the direction of the magnetic field is in the opposite direction of PM's field (Fig.5c).

Table1. Physical characteristics of main parts for numerical analysis

Items	Magnetic Specifications	Values
Permanent magnet (NdFeB)	Relative permeability	1
	Hc (kA/m)	1000
	Br (T)	1.4
Copper coil	Relative permeability	1
Nickel	Relative permeability	350
Air	Relative permeability	1
Galfenol (bimetal)	Relative permeability	250
Stainless steel (bimetal)	Relative permeability	1
Iron	Relative permeability	1500

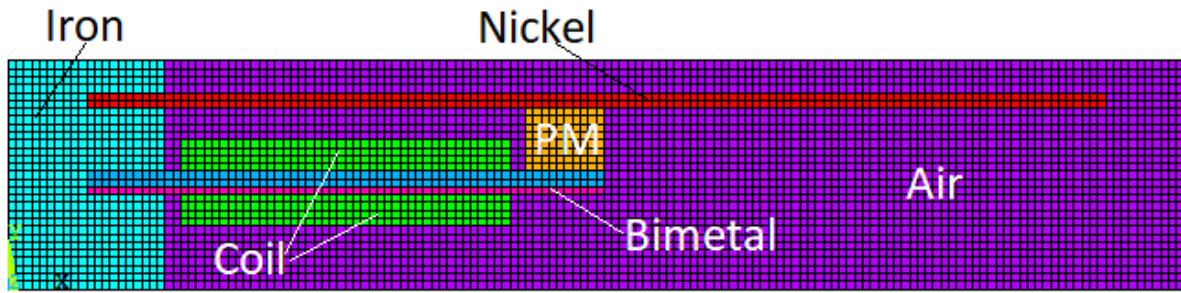


Fig. 4. 2D mesh of the anti-vibration system

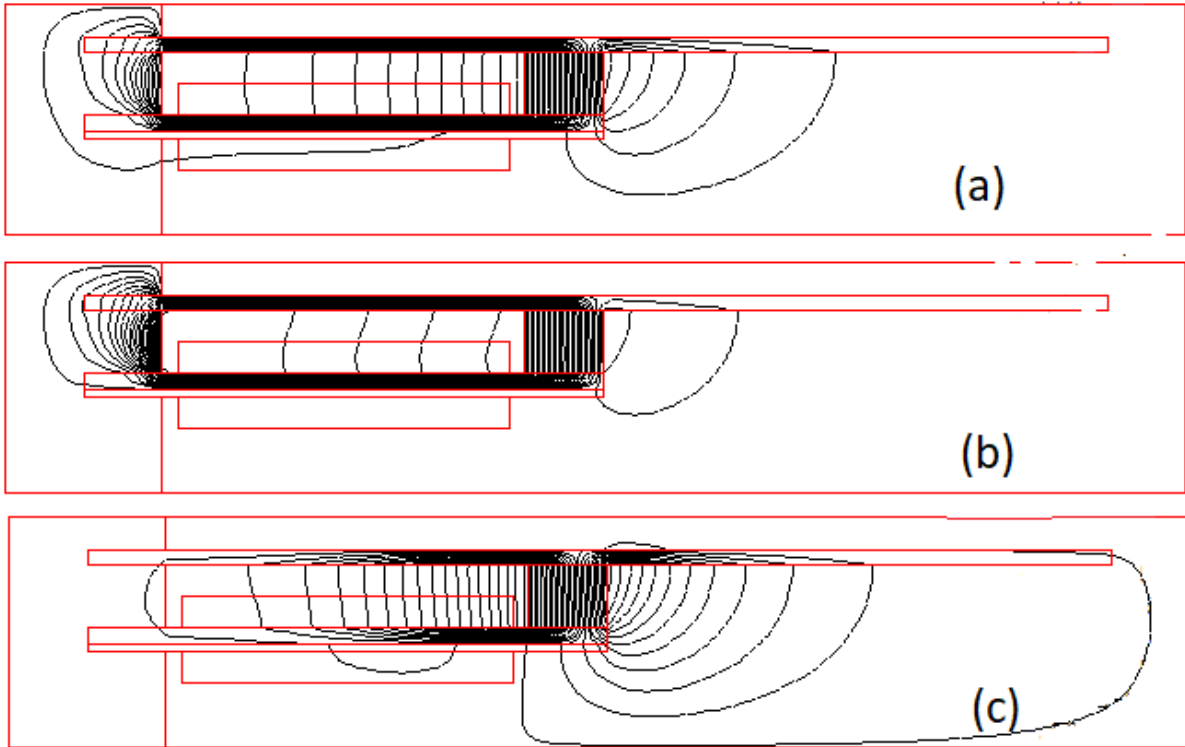


Fig. 5. 2D magnetic flux (a) only PM with no exciting coil; **normal** field (b) excitation coil with the magnetic field at the same direction of PM's field; **strong** field (c) excitation coil with the magnetic field at the opposite direction of PM's field; **weak** field

3. Experimental Setup and Data-Driven Modelling

3.1 Experimental setup

The experimental setup shown in Fig. 6, consists of three main components (1) cantilever beam with an unbalanced rotating mass at the tip, (2) LK-H05 laser displacement sensor, and (3) a bimetal actuator produced by authors connected to the main cantilever beam by a permanent magnet. The cantilever beam can be excited at different frequencies as the voltage supplied to the unbalanced rotating mass system varies.

To generate disturbance, the unbalanced rotating mass system is energized by a variable voltage that is corresponding to vibration with frequencies from 10 to 90 Hz. The deflection made by the unbalanced rotating mass system (resembling environmental forces) can be reduced by a well-manipulated counteracting force applied by the bimetal actuator (Fig. 7). A control system manipulates the actuator force to serve this purpose. The laser sensor measures the displacement at the tip of the beam and feeds it to a computer through an Advantech, PCI-1710 U/I/O card. A controller within the computer uses the measures signal and sends a command to a linear power amplifier, AETECTORN (model 7114), through the I/O card. Then, the amplifier provides an electrical current to the bimetal actuator accordingly. MATLAB/Simulink (particularly Real-Time Desktop toolbox) was

used for the implementation of the aforementioned control system. However, the system suffers from a technical limitation as the output signal of the I/O card can only have a positive range ([0-10] V). To resolve this issue, the controller was designed so that its output remains in the range of [-5 +5], then the output signal of the controller is added by 5 within the computer, so the input command to the I/O card varies within the range of [0 10]. Then, after the I/O card and before the amplifier, the voltage signal, which is in the range of [0 10] V, is shifted down by 5V. As a result, the negative part of the control command is practically covered. Since the unbalanced rotating mass system is a non-ideal source of vibration, it is a good source to examine the performance of the employed controller. The bimetal's coil is excited by an amplified signal with different frequencies (Fig. 8).

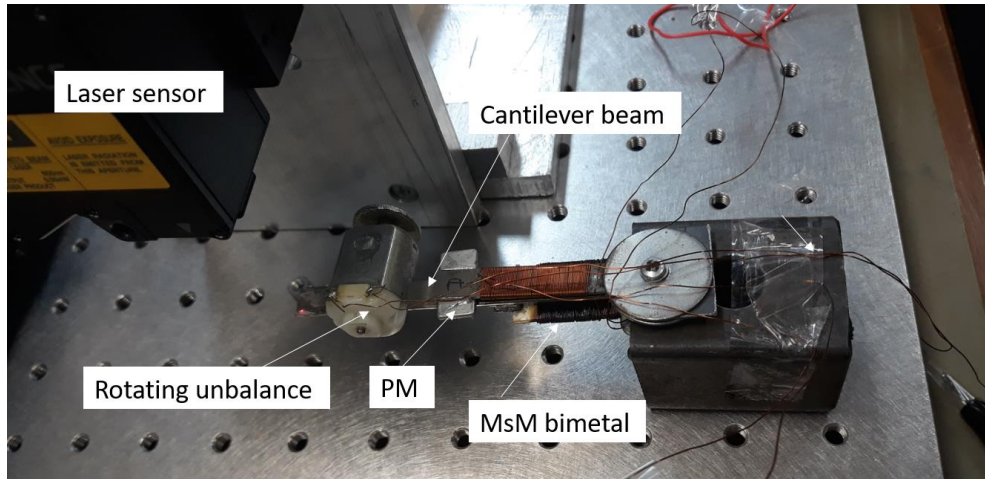
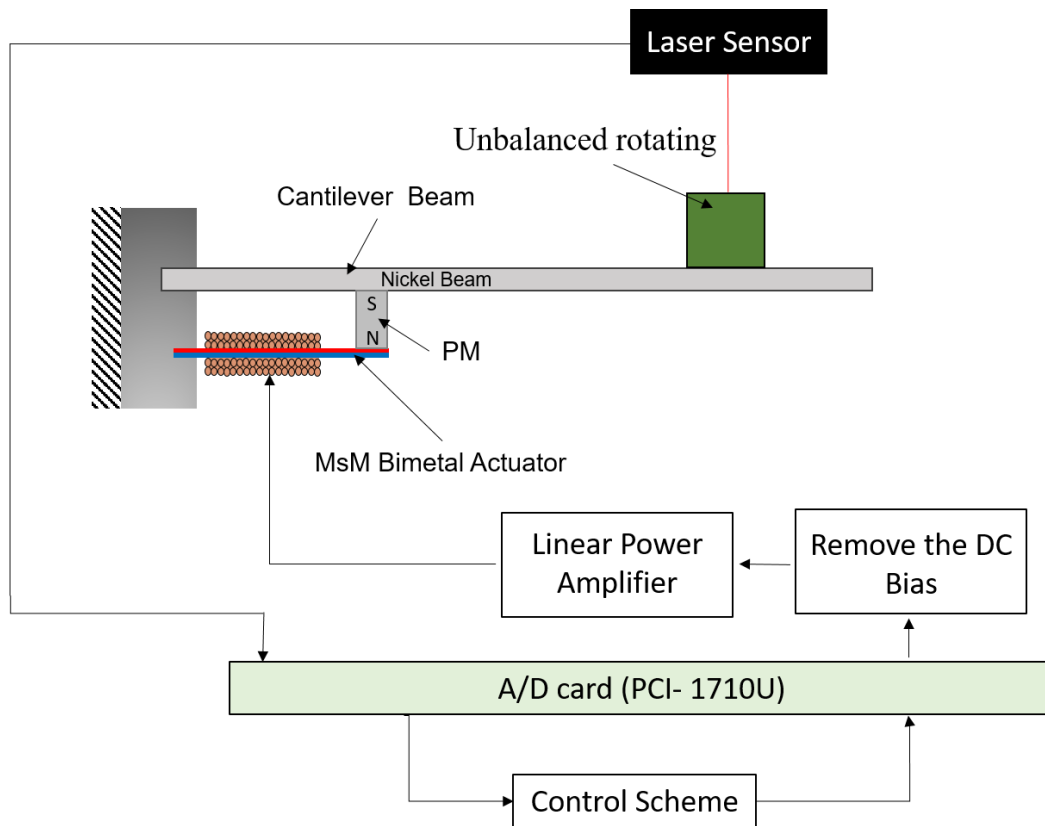
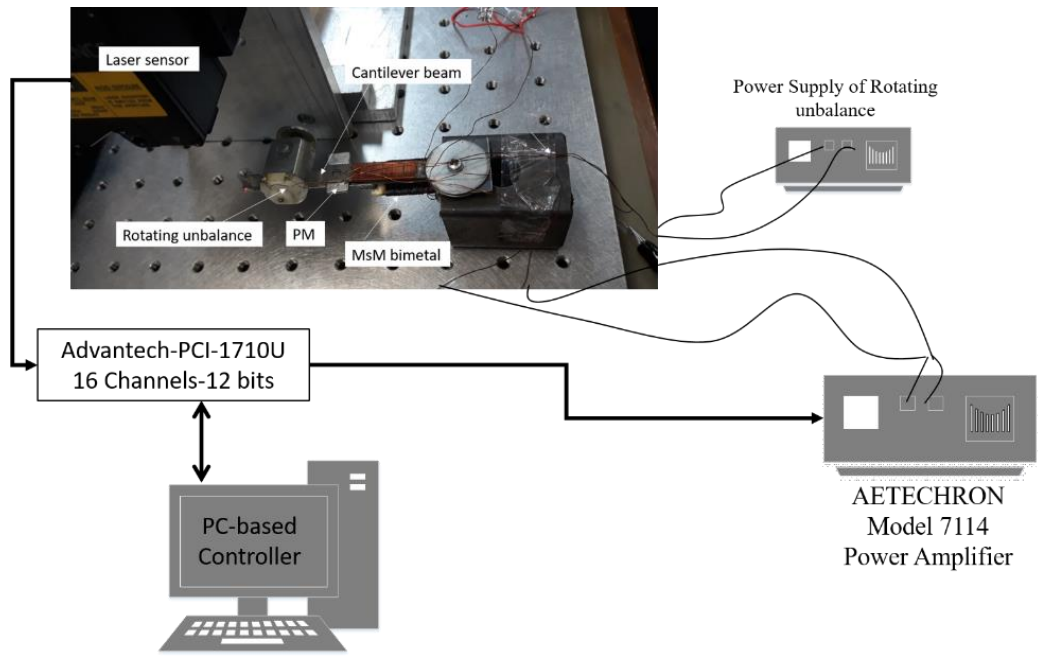


Fig. 6: Fabricated anti-vibration system



(a)



(b)

Fig.7. The anti-vibration system (a) schematic (b) real configuration

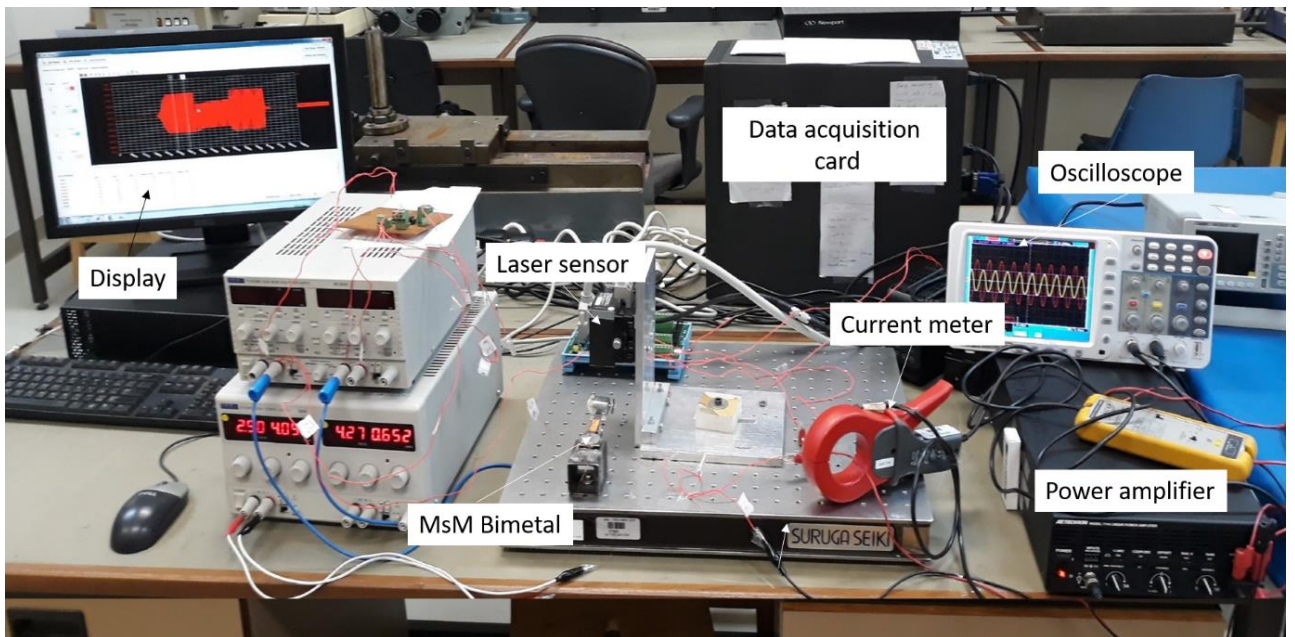


Fig.8. The real active control system

3.2. Impulse response analysis

By considering the vibrating compound (the beam, the motor, and the bimetal) cantilever beam as a single DOF system, its damping ratio can be measured easily from Eq. (22) [50].

$$r_{ext} = 2\zeta m_{eq} \omega_n, \quad \zeta = \frac{1}{\sqrt{1 + \left(\frac{2\pi}{\delta}\right)^2}}, \quad (22)$$

where

$$\delta = \ln \frac{x(t)}{x(t + T_d)}, \quad (23)$$

and T_d is the period of damped vibration. Figure 9 represents the tip displacement of the beam against time when excited by an impulse. The damping ratio of the cantilever beam can be calculated easily using this figure. T_d is about 14 ms and the two successive amplitudes are 0.049 and 0.043. From Eq. (22) and (23), the damping ratio and r_{ext} of the cantilever beam, are calculated as 0.02 and 0.538, respectively. Since the Nickel beam is annealed, we considered a small value of 0.01 for internal damping ($r_{int}=0.01$). The damping ratio is very small and therefore, the natural frequency of the magnetostrictive bimetal is very close to the damped frequency and can be calculated as:

$$\omega_n = \frac{\omega_d}{\sqrt{1 - \xi^2}} = \frac{448.8}{\sqrt{1 - 0.02^2}} = 448.89 \left(\frac{rad}{s} \right). \quad (24)$$

The mass of the beam m is of 25.2 gr, and the attached unbalanced rotating M_m is 20.4 gr. Hence, the equivalent mass m_{eq} of the cantilever beam can be approximated as [52]:

$$m_{eq} = \frac{33}{140} M_m + m = \frac{33}{140} 20.4 + 25.2 = 30 \text{ gr}, \quad (25)$$

and consequently equivalent bending rigidity EI is found as:

$$\omega_n = \sqrt{\frac{K}{m_{eq}}} = \sqrt{\frac{3EI_{eq}}{30 \times l^3}} \Rightarrow EI_{eq} = 1.47 \text{ N.m}^2 \quad (26)$$

The calculated EI is assumed as the equivalent EI of the vibrating compound. Table 2 shows a summary of values of all parameters measured in the setup.

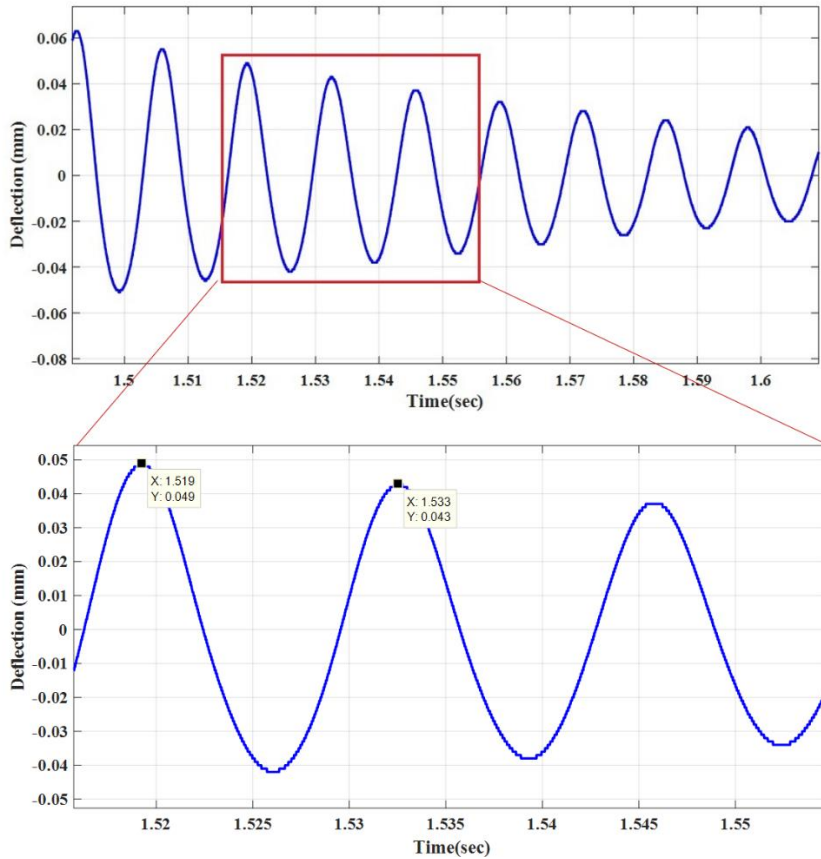


Fig. 9: Natural frequency measurement of the vibrating components using impulse response

Table 2. Parameters of the anti-vibration system

Parameter	Value
L (total length of the cantilever beam)	90 mm
Impedance of Bimetal excitation coil @60Hz	1.39 Ω
Inductance of Bimetal excitation coil @60Hz	44.8 mH
Bimetal excitation coil turns	90 turns
Bimetal excitation coil diameter	0.3 mm
$EI_{equivalent}$	1.47 N.m ²
r_{int} (internal damping coefficient)	0.010
r_{ext} (external damping coefficient)	0.005
μ (The effective mass of magnetostrictive bimetal per unit length)	0.1644 kg/m
Permendur relative permeability μ^σ	600
l_r (position of an applied force by unbalanced rotating)	75 mm
l_b (position of an applied force by bimetal)	30 mm
l_a (position of laser point)	89 mm
ω_n <i>Experimental</i> : Measured natural frequency of cantilever beam	71.44 Hz
ω	64 Hz

3.3. System Identification

To design an appropriate control system, it is vital to identify the dynamic behaviour of the vibrating compound, a combination of the beam, the unbalanced rotating mass system, and the bimetal actuator. This combination is considered as a simple one DOF mass-spring-damper system. The vibrating compound is energized through the bimetal's coil (input signal) $u(t)$, and the deflection of the beam $y(t)$ is considered as the output of the system. The bimetal's coil is excited by the signal generated by the function generator after being amplified by the linear power amplifier (AETECTORN, model 7114). The unbalance rotating mass system does not rotate during the experiments reported in this subsection. The gain value of the linear amplifier is set to be 10, similar to all other experiments reported in this research. The coil is energized with sinusoidal current functions with a constant current amplitude of 1A and at sixteen different frequencies from 10 to 90 Hz. The vibrating compound, assumed as a mass-spring-damper system, has the transfer function of s suits Eq. (27 and 28)

$$Y(s) = G(s)U(s), \quad (27)$$

$$G(s) = \frac{P}{s^2 + 2\xi\omega_n s + \omega_n^2}, \quad (28)$$

where, $Y(s)$ and $U(s)$ are the Laplace transform of output (beam tip displacement) $u(t)$ and input (the excitation current of the bimetal) $y(t)$, respectively.

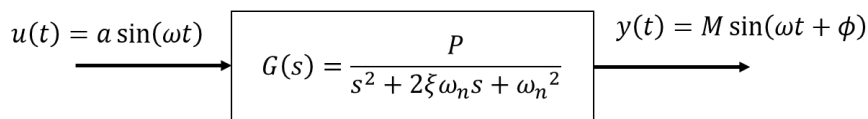


Fig. 10. The transfer function of the vibrating compound

Figure 10 shows the input and output of any single-input single-output linear system, such as the vibrating compound of this research, where the magnitude M and phase ϕ follow [53]

$$\begin{cases} M(\omega) = |G(s)|_{s=j\omega}, \\ \phi(\omega) = \angle G(s)_{s=j\omega}. \end{cases} \quad (29)$$

Calculation of $M(\omega)$, with the use of Eq.(29), of the transfer function of Eq. (28), leading to Eq.(30):

$$AM^2\omega^2 + BM^2 + C = -M^2\omega^4, \quad (30)$$

where $\omega_n^2 = -2\omega_n^2 + 4\xi^2\omega_n^2$, $B = -\omega_n^4$ and $C = -P^2$. Since the amplitude of the tip displacement and bimetal excitation current are known (can be measured via experiments), M is known at each exciting frequency ω energized the coil in this experiment. All these sixteen pairs of M and ω are used to find three unknowns of A , B , and C . To do so, Eq. (30) are written for all sixteen frequencies with known M to obtain Eq. (31) which returns A , B , and C .

$$\begin{bmatrix} M_1^2\omega_1^2 & M_1^2 & 1 \\ \vdots & \vdots & \vdots \\ M_{16}^2\omega_{16}^2 & M_{16}^2 & 1 \end{bmatrix} \begin{bmatrix} A \\ B \\ C \end{bmatrix} = \begin{bmatrix} -M_1^2\omega_1^4 \\ \vdots \\ -M_{16}^2\omega_{16}^4 \end{bmatrix} \quad (31)$$

Eq.(31) can be optimally solved using the Least Square of Errors (LSE) method [54]. Triple unknown parameters of Eq. (28), found with the use of obtained A , B , and C from (31), result in Eq. (32), where (^) refers to estimation. That is Eq. (32) provides an estimation of the real transfer function of Eq. (28).

$$\hat{G}(s) = \frac{3.08 \times 10^6}{s^2 + 41.52s + 2.052 \times 10^5} \quad (32)$$

Figure 11 shows the amplitude of beam tip displacement versus bimetal excitation frequency both for the experimental results and the identified model. A good agreement is seen between the experimental dynamic behavior of the vibrating compound and the corresponding behavior predicted by the identified model via Eq. (32).

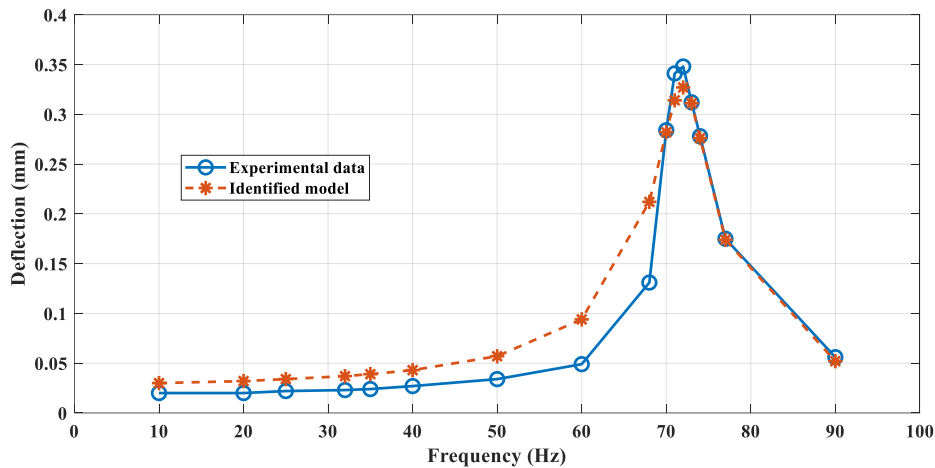


Fig. 11. Frequency response of the vibrating compound

4. Control Scheme

There are several types of control schemes employed in anti-vibration systems. All try to retain the vibration amplitude of the main structure at the minimum possible level. Moon *et al.* proposed a linear quadratic feedback controller for a linear magnetostrictive actuator in a real-time application and can reduce displacement and acceleration in the first four modes by at least 75% [55]. Bian *et al.* incorporated a multi-mode adaptive positive position feedback algorithm and feedforward compensator and used it as the controller to enhance the effectiveness of vibration suppression [56, 57].

In this research and many similar works, the objective of vibration attenuation is to reduce the displacement caused by an external vibration source towards zero. This displacement is a disturbance in terms of control, the effect of a non-manipulated cause (i.e. external vibration). Feedforward methods are widely employed to reject disturbance [58, 59]. However, these methods need disturbance dynamics or the relationship between external non-manipulated cause and the disturbance. Although, it is possible to identify such a relationship in lab environment, where the disturbance is artificially generated (e.g. with an unbalanced motor); in reality (e.g. the effect of wind), such a relationship is extremely hard to be found. As a matter of novelty, this paper presents a control scheme, which rejects the effect of any unknown disturbance. In this research, to have a general method, the displacement caused by the external vibration source (the unbalanced rotating mass system) is seen as an unknown disturbance, d .

The aforementioned novel control scheme is presented in Fig. 12, with a reference or desired tip displacement of r , which equals zero in this research. The open-loop system includes the vibrating compounds (the bimetal, the beam, and the unbalanced motor). The G transfer function of the vibrating compound, presented in Eq. (28), relating the bimetal current u to the beam tip displacement, while the unbalance does not rotate, i.e. there is no disturbance ($d=0$). y and y_p represent displacement with and without the effect of the disturbance, respectively. In subsection 3-2, y and y_p were equal in absence of the disturbance.

Components peculiar to the closed-loop control system are: (1) $C(s)$, the controller, (2) $\hat{G}(s)$, Eq.(32) and an approximation of Eq.(28), which estimates y_p based on u , and (3) $\hat{G}_{in}(s)$, a realizable approximate inverse of $G(s)$. This component contributes to the removal of disturbance from the closed-loop system dynamics.

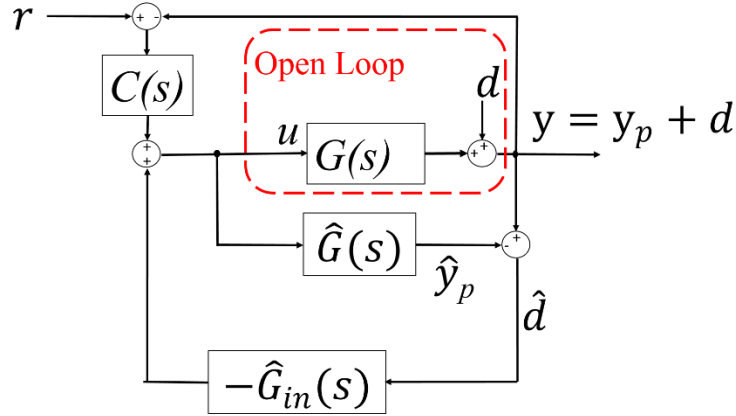


Fig. 12. The control scheme of the anti-vibration system

Ideally, $\hat{G}(s) = G(s)$ and $\hat{G}_{in}(s) \times G(s) = 1$. In such an ideal situation, $\hat{y}_p = u\hat{G}(s) = uG(s) = y_p$; therefore, $\hat{d} = y_p + d - \hat{y}_p = y_p + d - y_p = d$. As a result

$$u(s) = C(s)(r(s) - y(s)) - \frac{d(s)}{G(s)}. \quad (33)$$

With such a control law, in an ideal situation, $y(s) = G(s)u(s) = G(s) \left(C(s)(r(s) - y(s)) - \frac{d(s)}{G(s)} \right) + d(s)$; thus,

$$y(s) = C(s)G(s)(r(s) - y(s)). \quad (34)$$

Eq. (34) represents a simple feedback control system, as shown in Fig. 13, where the reference, i.e. the desired displacement, is zero. That is, the effect of disturbance is canceled, ideally, as if it does not exist. A P-action feedback controller or gain of K_P was chosen for the control system, or $C(s)=K_P$. With the use of equation (32), the closed-loop transfer function of the control loop presented in Fig.12 is developed as Eq.(35):

$$G_{CL}(s) = \frac{y(s)}{r(s)} = \frac{3.08 \times 10^6 \times K_P}{s^2 + 41.52s + (20.52 + 3.08 \times K_P) \times 10^5}. \quad (35)$$

For any K_P larger than 0.0053, both poles of the closed-loop system are complex, and their real value is -20.76. Such a negative real value of poles, considerably far from zero, shows the stability of the control system. The fact that the closed loop system is always complex means that oscillations/vibrations will be still there, even at low amplitudes of disturbance. The higher gain, the higher absolute value of the imaginary part of the closed poles, the higher frequency of oscillation. As high frequency vibration demands relatively high energy and fades faster, the higher values of control gain will better attenuate the unwanted disturbance. By the way, inaccuracies in the identification of $\hat{G}(s)$, particularly due to nonlinearities, may diminish the performance of this control system.

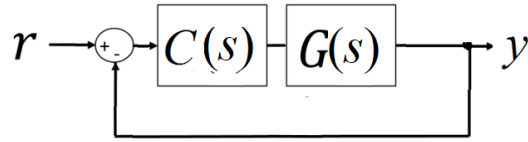


Fig. 13. The equivalent of the control system presented in Fig.11 at ideal situation

The last step to clarify the control system presented in Fig.13 is to develop $\hat{G}_{in}(s)$, equivalent to an inverse of $\hat{G}(s)$, Eq.28, in which its inverse is not proper and realizable. In a proper transfer function, the order of the denominator is higher than or equal to the order of the numerator. To assure properness, terms of $(1 - s/p_i)^3$ are multiplied to the denominator of an improper transfer function to increase its order, p_i is a stable pole much further from 0 than existing poles of the transfer function. In this research three identical p_i of -10 were added to the inverse of $\hat{G}(s)$ to develop $\hat{G}_{in}(s)$:

$$\hat{G}_{in}(s) = -\frac{s^2 + 41.52s + 2.052 \times 10^5}{3.08 \times 10^6(1 + 0.1s)^3}$$

5. Results and Discussion

Figure 14 shows the amplitude of the vibration on the tip of the cantilever beam in the absence of a control system. The nominal amplitude of vibration varies from 550 to 650 μ m. To investigate the effect of the control system (Fig. 15), gains of 0.15, 0.25, 0.5, and 0.75 are used instead of $C(s)$. The attenuation percentage increases with the gain value; however, the energizing current of the bimetal increases too much. Therefore, based on the current density limitation, it was found that the maximum implementable value of controller gain is 0.75. As an example, Fig. 16 shows that the low controller gain of 0.15 attenuates the vibration by about 14.9%, while this attenuation reaches 33.6% with a gain of 0.75. Frequency response without and with the control system with gains of 0.15 and 0.5 are presented in Figs. 16 and 17, respectively. Comparing Figs. 16 and 17 confirm that a higher gain value causes a higher attenuation rate. Furthermore, the proposed anti-vibration system is particularly suitable to attenuate the effect of external disturbance on beam displacement in frequencies between 55 Hz to 90 Hz. As mentioned in section 4, the proposed control scheme uses no knowledge of disturbance dynamics. Hence, it is not comparable to methods that control known disturbances. As an idea for future investigations, the proposed $C(s)$ may be chosen as a PID designed with a robust control technique, e.g H_∞ , to possibly compensate inaccuracy in the identification of $G(s)$ to some extent. By the way, even with the suggested approach, dynamic cancellations leading to (34) will remain imperfect due to model inaccuracy.

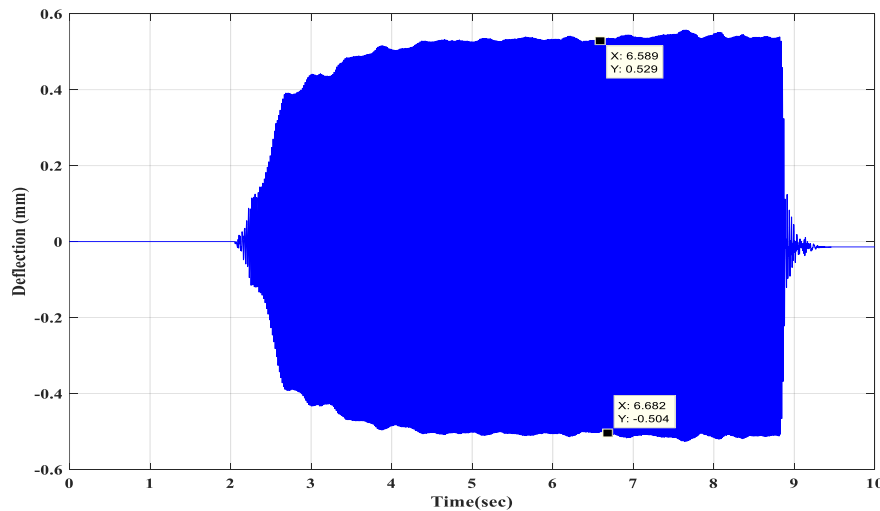
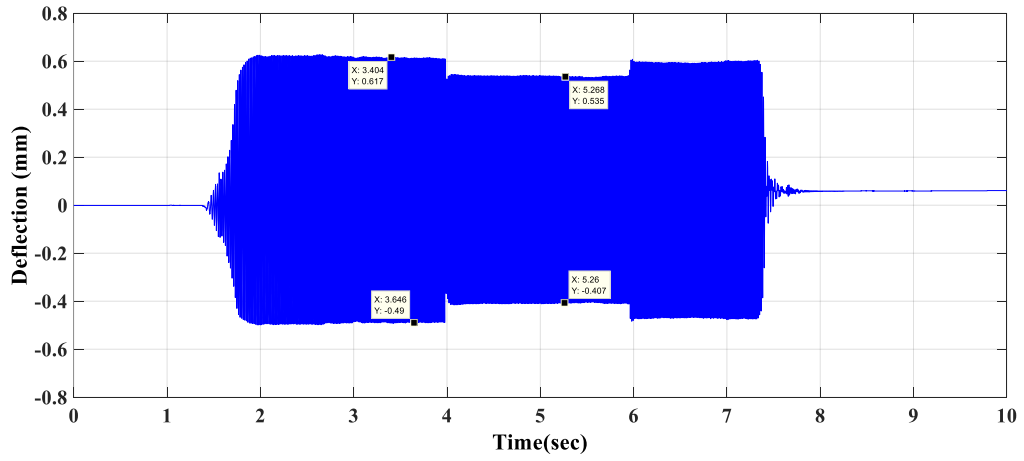
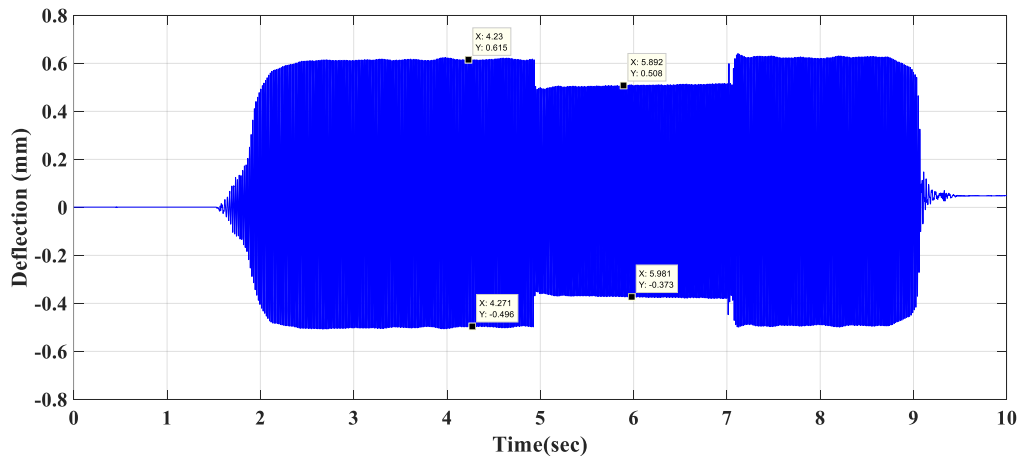


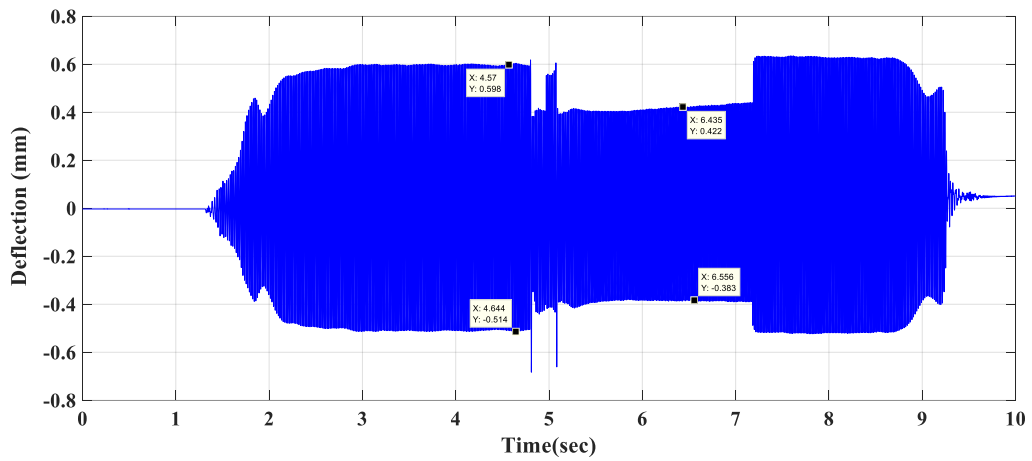
Fig. 14: Displacement of the beam tip without any input signal, driving voltage of the motor is 2.5 V, driving frequency of the unbalanced rotating is 63 Hz,



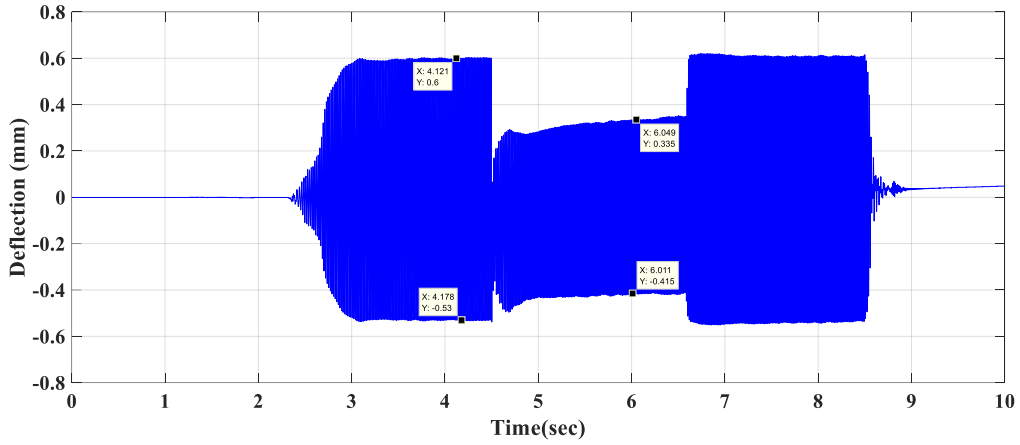
(a) Gain=0.15



(b) Gain=0.25



(c) Gain=0.5



(d) Gain=0.75

Figure 15. Beam tip displacement with and without the control system with different controller gains. The system is subject to control in the time range of [4.5 6.5] s

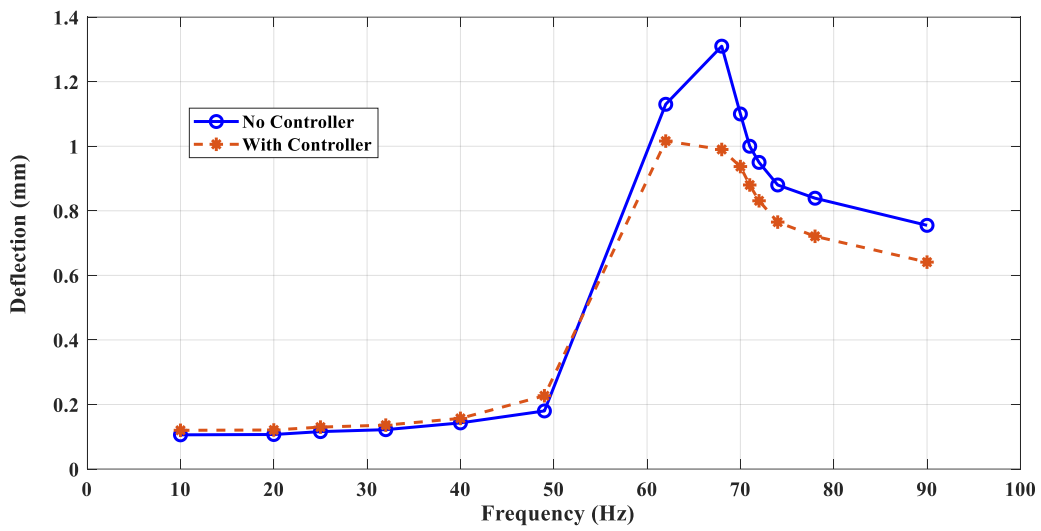


Fig. 16. Beam tip displacement in the frequency domain with no control and with FF controller with $G_c=0.15$

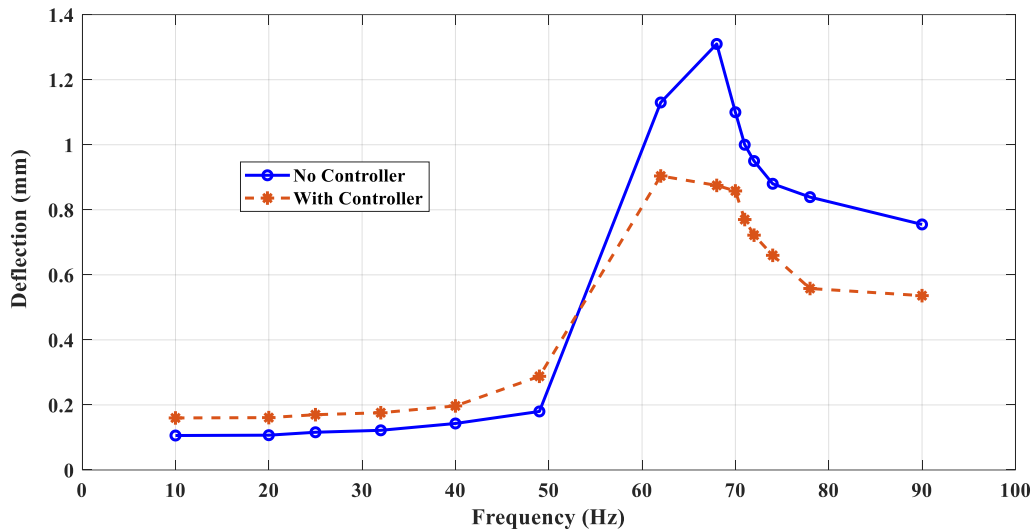


Fig. 17: Frequency response of the vibrational system with and without the control system with a controller gain of 0.5

6. Conclusions

This paper presents a new active anti-vibration system using a magnetostrictive bimetal actuator. This system was employed to reduce the effect of unwanted external vibrations on a cantilever beam. The proposed method has two advantages over existing similar systems: (1) use of magnetostrictive bimetal actuator without employing temperature sensor and any recalibration processes, and (2) it can suppress vibrations without knowing the details of external vibrations (disturbance) and their source. To simulate an unwanted environmental vibration, an unbalanced rotating mass system was mounted to the tip of the beam; however, its information was not used in the design of the control system as the method has been designed to attenuate any unknown external vibration. In the first step, the principles of this anti-vibration system were explained. Then, an approximate analytical model was developed for a beam subject to the proposed control system and external vibration. Afterward, the impulse response of the combination of the beam, the unbalanced motor, and the bimetal (vibrating compound, in this paper) was investigated, while the unbalance did not rotate. At the next stage, an empirical model of the vibrating compound (again with non-rotating unbalance) was developed. A very good agreement between experimental results and the identified model was achieved, which proves the model can predict the dynamic behaviour of the vibrating compound. Finally, an innovative control system including three components was designed, analysed, and implemented, which demonstrates the capability of about 33.6 % reduction in vibration amplitude of the main system (the beam vibration amplitude).

References

- [1] F. Resta, F. Ripamonti, G. Cazzulani, M. Ferrari, Independent modal control for nonlinear flexible structures: An experimental test rig, *Journal of Sound and Vibration*, 329 (2010) 961-972.
- [2] Y. Liu, W. Zhan, M. Xing, Y. Wu, R. Xu, X. Wu, Boundary Control of a Rotating and Length-Varying Flexible Robotic Manipulator System, *IEEE Transactions on Systems, Man, and Cybernetics: Systems*, (2020).
- [3] A. Özer, S.E. Semercigil, R.P. Kumar, P. Yowat, Delaying tool chatter in turning with a two-link robotic arm, *Journal of Sound and Vibration*, 332 (2013) 1405-1417.
- [4] L. Yu, C. Xiongbin, M. Yanfang, W. Yilin, Observer-based boundary control for an asymmetric output-constrained flexible robotic manipulator, *SCIENCE CHINA Information Sciences*, (2020).
- [5] D. Ning, S. Sun, H. Li, H. Du, W. Li, Active control of an innovative seat suspension system with acceleration measurement based friction estimation, *Journal of Sound and Vibration*, 384 (2016) 28-44.
- [6] L. Zhang, J. Tao, X. Qiu, Active control of transformer noise with an internally synthesized reference signal, *Journal of Sound and Vibration*, 331 (2012) 3466-3475.

- [7] H. Ma, J. Wu, L. Yang, Z. Xiong, Active chatter suppression with displacement-only measurement in turning process, *Journal of Sound and Vibration*, 401 (2017) 255-267.
- [8] S. Yavari, M. Modabberifar, M.R. Sheykhleslami, An experimental investigation of electro discharge machining parameters effects on ferromagnetic properties of extra-low-carbon steel, *Journal of Magnetism and Magnetic Materials*, (2022) 169041.
- [9] J. Teter, G.C. Horner, L. Bromberg, Precision cryogenic magnetostrictive actuator using a persistent high TC magnet, *Journal of Applied Physics*, 87 (2000) 6313-6315.
- [10] C. Fang, W. Wang, Introduction to Shape-Memory Alloys, in: *Shape Memory Alloys for Seismic Resilience*, Springer, 2020, pp. 1-41.
- [11] N. Keshtkar, S. Keshtkar, A. Poznyak, Deflection Sliding Mode Control of a Flexible Bar Using a Shape Memory Alloy Actuator with an Uncertainty Model, *Applied Sciences*, 10 (2020) 471.
- [12] S.-C. Kwon, H.-U. Oh, Passive micro-jitter isolation of gimbal-type antenna by using a superelastic SMA gear wheel, *Mechanical Systems and Signal Processing*, 114 (2019) 35-53.
- [13] Y. Liu, F. Guo, X. He, Q. Hui, Boundary control for an axially moving system with input restriction based on disturbance observers, *IEEE Transactions on Systems, Man, and Cybernetics: Systems*, 49 (2019) 2242-2253.
- [14] M.A. Miller, Camera lens suspension with limiter, in, Google Patents, 2018.
- [15] T. Shiraishi, H. Misaki, Vibration Control by a Shear Type Semi-active Damper Using Magnetorheological Grease, *Journal of Physics*, 744 (2016).
- [16] V. Mikhailov, A. Bazinenkov, A. Kazakov, Active vibration isolation of nanotechnology equipment, in: *IOP Conference Series: Materials Science and Engineering*, IOP Publishing, 2020, pp. 044046.
- [17] R.L. Harne, Z. Deng, M.J. Dapino, Adaptive magnetoelastic metamaterials: A new class of magnetorheological elastomers, *Journal of Intelligent Material Systems and Structures*, 29 (2018) 265-278.
- [18] B. Kavlicoglu, Y. Liu, B. Wallis, H. Sahin, M. McKee, F. Gordaninejad, Two-way controllable magnetorheological elastomer mount for shock and vibration mitigation, *Smart Materials and Structures*, 29 (2020) 024002.
- [19] W. Xu, Y. Wu, Piezoelectric actuator for machining on macro-to-micro cylindrical components by a precision rotary motion control, *Mechanical Systems and Signal Processing*, 114 (2019) 439-447.
- [20] L. Wei, Z. Mengde, W. Zhengquan, Y. Zhuang, L. Yu, W. Shihong, C. Xiaochun, L. Xiao, B. Liang, J. Zhenyuan, An active damping vibration control system for wind tunnel models, *Chinese Journal of Aeronautics*, 32 (2019) 2109-2120.
- [21] J.-j. Wei, Z.-c. Qiu, Y.-c. Wang, Experimental comparison research on active vibration control for flexible piezoelectric manipulator using fuzzy controller, *Journal of Intelligent and Robotic Systems*, 59 (2010) 31-56.
- [22] S.M. Savaresi, C. Poussot-Vassal, C. Spelta, O. Sename, L. Dugard, *Semi-active suspension control design for vehicles*, Elsevier, 2010.
- [23] W. Larbi, J.-F. Deü, Reduced order finite element formulations for vibration reduction using piezoelectric shunt damping, *Applied Acoustics*, 147 (2019) 111-120.
- [24] R. Darleux, B. Lossouarn, J.-F. Deü, Passive self-tuning inductor for piezoelectric shunt damping considering temperature variations, *Journal of Sound and Vibration*, 432 (2018) 105-118.
- [25] L. Dal Bo, P. Gardonio, D. Casagrande, S. Saggini, Smart panel with sweeping and switching piezoelectric patch vibration absorbers: Experimental results, *Mechanical Systems and Signal Processing*, 120 (2019) 308-325.
- [26] H. He, X. Tan, J. He, F. Zhang, G. Chen, A novel ring-shaped vibration damper based on piezoelectric shunt damping: Theoretical analysis and experiments, *Journal of Sound and Vibration*, 468 (2020) 115125.
- [27] S. Kapuria, M.Y. Yasin, Active vibration control of piezoelectric laminated beams with electroded actuators and sensors using an efficient finite element involving an electric node, *Smart Materials and Structures*, 19 (2010) 045019.

- [28] I. Bruant, L. Gallimard, S. Nikoukar, Optimal piezoelectric actuator and sensor location for active vibration control, using genetic algorithm, *Journal of Sound and Vibration*, 329 (2010) 1615-1635.
- [29] V. Gupta, M. Sharma, N. Thakur, S. Singh, Active vibration control of a smart plate using a piezoelectric sensor–actuator pair at elevated temperatures, *Smart Materials and Structures*, 20 (2011) 105023.
- [30] H. Hoshyarmanesh, M. Ghodsi, M. Kim, H.H. Cho, H.-H. Park, Temperature Effects on Electromechanical Response of Deposited Piezoelectric Sensors Used in Structural Health Monitoring of Aerospace Structures, *Sensors*, 19 (2019) 2805.
- [31] D. Williams, H. Haddad Khodaparast, S. Jiffri, C. Yang, Active vibration control using piezoelectric actuators employing practical components, *Journal of Vibration and Control*, 25 (2019) 2784-2798.
- [32] H. Hoshyarmanesh, N. Nehzat, M. Salehi, M. Ghodsi, H.-S. Lee, H.-H. Park, Piezoelectric Transducers on Curved Dispersive Bending Wave and Poke-Charged Touch Screens, *Materials and Manufacturing Processes*, 29 (2014) 870-876.
- [33] P. Pillatsch, B. Xiao, N. Shashoua, H. Gramling, E. Yeatman, P. Wright, Degradation of bimorph piezoelectric bending beams in energy harvesting applications, *Smart Materials and Structures*, 26 (2017) 035046.
- [34] M. Ghodsi, T. Ueno, H. Teshima, H. Hirano, T. Higuchi, E. Summers, “Zero-power” positioning actuator for cryogenic environments by combining magnetostrictive bimetal and HTS, *Sensors and Actuators A: Physical*, 135 (2007) 787-791.
- [35] M. Ghodsi, M. Modabberifar, T. Ueno, Quality factor, static and dynamic responses of miniature galferol actuator at wide range of temperature, *International Journal of Physical Sciences*, 6 (2011) 8143-8150.
- [36] S.Z. Nkeutia, V.K. Tamba, P.K. Talla, Hysteretic dynamics inducing coexistence of attractors in a thin magnetostrictive actuator system with quintic nonlinearity, *Journal of Magnetism and Magnetic Materials*, 507 (2020) 166858.
- [37] S. Talebian, Y. Hojjat, M. Ghodsi, M.R. Karafi, Study on classical and excess eddy currents losses of Terfenol-D, *Journal of Magnetism and Magnetic Materials*, 388 (2015) 150-159.
- [38] S. Talebian, Y. Hojjat, M. Ghodsi, M.R. Karafi, S. Mirzamohammadi, A combined Preisach–Hyperbolic Tangent model for magnetic hysteresis of Terfenol-D, *Journal of Magnetism and Magnetic Materials*, 396 (2015) 38-47.
- [39] M. Ghodsi, S. Mirzamohammadi, S. Talebian, Y. Hojjat, M. Sheikhi, A. Al-Yahmedi, A. Özer, Analytical, numerical and experimental investigation of a giant magnetostrictive (GM) force sensor, *Sensor Review*, 35 (2015) 357-365.
- [40] S. Mirzamohammadi, M.M. Sheikhi, M.R. Karafi, M. Ghodsi, S. Ghorbanirezaei, Novel Contactless Hybrid Static Magnetostrictive Force-Torque (CHSMFT) Sensor Using Galferol, *Journal of Magnetism and Magnetic Materials*, (2022) 168969.
- [41] M. Ghodsi, T. Ueno, T. Higuchi, Novel Magnetostrictive Bimetal Actuator Using Permendur, *Advanced Materials Research*, 47-50 (2008) 262-265.
- [42] M. Ghodsi, N. Hosseinzadeh, A. Ozer, H.R. Dizaj, Y. Hojjat, N.G. Varzeghani, M.R. Sheykholeslami, S. Talebian, M.H. Ghodsi, A. Al-Yahmedi, Development of Gasoline Direct Injector Using Giant Magnetostrictive Materials, *IEEE Transactions on Industry Applications*, 53 (2017) 521-529.
- [43] M. Brennan, J. Garcia-Bonito, S. Elliott, M. Dadkhah, R.J.S.m. Pinnington, Experimental investigation of different actuator technologies for active vibration control, *J Smart materials and Structures*, 8 (1999) 145-153.
- [44] H.M. Zhou, X.J. Zheng, Y.-H.J.S.m. Zhou, structures, Active vibration control of nonlinear giant magnetostrictive actuators, 15 (2006) 792.
- [45] Z.J. Geng, L.S.J.I.T.o.c.s.t. Haynes, Six degree-of-freedom active vibration control using the Stewart platforms, 2 (1994) 45-53.
- [46] M. Ahanpanjeh, M. Ghodsi, Y. Hojjat, Precise Positioning of Terfenol-D Actuator by Eliminating the Heat Generated by Coil, *Modern Applied Science*, 10 (2016) p232.

- [47] M. Ghodsi, A. Saleem, A. Özer, I. Bahadur, K. Alam, A. Al-Yahmadi, M.H. Ghodsi, H. Hoshyarmanesh, M.R. Sheykholeslami, Elimination of thermal instability in precise positioning of Galfenol actuators, in: Behavior and Mechanics of Multifunctional Materials and Composites 2016, International Society for Optics and Photonics, 2016, pp. 980008.
- [48] A. Nyman, Control devices employing magnetostrictive materials, in, Google Patents, 1969.
- [49] A.E. Clark, M. Wun-Fogle, J.B. Restorff, Bimetallic strips for energy harvesting, actuation and sensing, in, Google Patents, 2011.
- [50] M. Ghodsi, H. Ziaiefar, M. Mohammadzaheri, A. Al-Yahmedi, Modeling and characterization of permendur cantilever beam for energy harvesting, Energy, 176 (2019) 561-569.
- [51] D. Tjepkema, J. van Dijk, H. Soemers, Sensor fusion for active vibration isolation in precision equipment, Journal of Sound and Vibration, 331 (2012) 735-749.
- [52] D.J. Inman, Engineering vibration, 4th ed., Pearson Education Limited, 2014.
- [53] K. Ogata, Modern Control Engineering, Prentice-Hall, Inc., Upper Saddle River, New Jersey, USA, 1997.
- [54] M. Mohammadzaheri, R. Tafreshi, Z. Khan, M. Ghodsi, M. Franchek, K. Grigoriadis, Modelling of petroleum multiphase flow in electrical submersible pumps with shallow artificial neural networks, Ships and Offshore Structures, 15 (2020) 174-183.
- [55] S.-J. Moon, C.-W. Lim, B.-H. Kim, Y.J.J.o.S. Park, Vibration, Structural vibration control using linear magnetostrictive actuators, 302 (2007) 875-891.
- [56] L. Bian, W. Zhu, Adaptive positive position feedback control with a feedforward compensator of a magnetostrictive beam for vibration suppression, Smart Materials and Structures, 27 (2018) 075037.
- [57] Y. Liu, Y. Fu, W. He, Q. Hui, Modeling and observer-based vibration control of a flexible spacecraft with external disturbances, IEEE Transactions on Industrial Electronics, 66 (2018) 8648-8658.
- [58] Q. Zhu, J.-Z. Yue, W.-Q. Liu, X.-D. Wang, J. Chen, G.-D. Hu, Active vibration control for piezoelectricity cantilever beam: an adaptive feedforward control method, smart materials and structures, 26 (2017) 047003.
- [59] X. Wang, Z. Gao, Y. Fang, J. Hu, X. Zhu, Active vibration control of smart flexible piezoelectric beam with a tip mass using hybrid FX-VSSLMS algorithm, The Journal of Engineering, 2019 (2019) 172-174.